

Mg, Al, Si, Ca, Ti, Fe, and Ni abundance for a sample of solar analogues

Ricardo López-Valdivia^{*}, Emanuele Bertone, and Miguel Chávez

Instituto Nacional de Astrofísica, Óptica y Electrónica, Luis Enrique Erro 1, Tonantzintla, Puebla, 72840, México

Accepted XXX. Received YYY; in original form ZZZ

ABSTRACT

We report on the determination of chemical abundances of 38 solar analogues, including 11 objects previously identified as super metal-rich stars. We have measured the equivalent widths for 34 lines of 7 different chemical elements (Mg, Al, Si, Ca, Ti, Fe, and Ni) in high-resolution ($\mathcal{R} \sim 80\,000$) spectroscopic images, obtained at the Observatorio Astrofísico Guillermo Haro (Sonora, Mexico), with the Cananea High-resolution Spectrograph. We derived chemical abundances using ATLAS12 model atmospheres and the Fortran code MOOG. We confirmed the super metallicity status of 6 solar analogues. Within our sample, BD+60 600 is the most metal-rich star ($[\text{Fe}/\text{H}] = +0.35$ dex), while for HD 166991 we obtained the lowest iron abundance ($[\text{Fe}/\text{H}] = -0.53$ dex). We also computed the so-called [Ref] index for 25 of our solar analogues, and we found, that BD+60 600 ($[\text{Ref}] = +0.42$) and BD+28 3198 ($[\text{Ref}] = +0.34$) are good targets for exoplanet search.

Key words: stars: solar-type; stars: abundances; techniques: spectroscopic.

1 INTRODUCTION

Stellar chemical composition represents an important parameter in stellar and galactic astronomy studies, and, in particular, in the relatively recent field of exoplanets. In this latter field, different studies have aimed at searching for possible correlations between properties (mainly chemical composition) of host stars and the occurrence of exoplanets. Gonzalez (1997), with the search for exoplanets still in its early stages, suggested a link between high metal content of host stars and the presence of giant gaseous planets. Such correlation was later confirmed by other authors (e.g., Fischer & Valenti 2005; Johnson et al. 2010; Sousa et al. 2011) and it agrees with the core accretion theory for planet formation (Pollack et al. 1996; Alibert, Mordasini & Benz 2004), where high metallicity facilitates the formation of giant gas planets.

Within this scenario, the iron abundance ($[\text{Fe}/\text{H}]$) is commonly used as proxy for overall metallicity; however, Gonzalez (2009) suggested the use of a new metallicity index, called [Ref], which takes into account the mass abundance of the refractory elements Mg, Si, and Fe, since their number densities and condensation temperatures are very similar. This [Ref] index is more sensitive (mainly at values greater than +0.20 dex) than $[\text{Fe}/\text{H}]$ to describe the incidence probability of giant planets orbiting a star (Gonzalez 2014).

The present work is the continuation of a global project aimed at determining atmospheric parameters and chemical abundances of solar analogues (main sequence stars with spectral types between G0 and G3)¹, with special interest in looking for giant exoplanet host star candidates. In López-Valdivia et al. (2014), we simultaneously determined the basic stellar atmospheric parameters [effective temperature (T_{eff}), surface gravity ($\log g$), and global metallicity ($[\text{M}/\text{H}]$)], for a sample of 233 solar analogues, using intermediate-resolution spectra ($\mathcal{R} \sim 1700$ at 4300 Å) and a set of Lick-like indices defined within 3800–4800 Å. We determined for the first time the atmospheric parameters for 213 stars, of which 20 are new super metal-rich star candidates (SMR; $[\text{M}/\text{H}] \geq 0.16$ dex).

The second goal of our project is the analysis of chemical abundances, which we started with the determination of the lithium abundance of a sample of 52 stars (López-Valdivia et al. 2015). The analysis was carried out using narrow band high-resolution spectra ($\mathcal{R} \sim 80\,000$) centred on the 6708 Å lithium feature. This sample included 12 SMR objects from our previous work (López-Valdivia et al. 2014).

In this third part of the series, we complement the lithium abundance with the chemical abundances of Mg, Al,

¹ In our sample the stars HD 130948 and HD 168874 have a different spectral type; nevertheless, we included them, because their atmospheric parameters are compatible with the rest of the sample.

^{*} E-mail: valdivia@inaoep.mx

Si, Ca, Ti, Fe, and Ni, for 38 solar analogues. The sample and the observations are described in Section 2. In Section 3, we detail the determination of the chemical abundances, and, in Section 4, we discuss the results.

2 STELLAR SAMPLE AND OBSERVATIONS

We selected 38 objects among the brightest stars of López-Valdivia et al. (2015). In Table 1, we list the name of the star, the visual magnitude, the spectral type and the atmospheric parameters (and their uncertainties) for the entire sample. The spectroscopic data were collected at the 2.1 m telescope of the Observatorio Astrofísico Guillermo Haro, located in Mexico, using the Cananea High-resolution Spectrograph (CanHiS). CanHiS is equipped with mid-band filters, that provide access to ~ 40 Å wide wavelength intervals in a single diffraction order.

We observed the entire sample with a spectral resolving power of $\mathcal{R} \sim 80\,000$ and a typical signal-to-noise ratio (S/N) of about 100, using 4 different filters of CanHiS, centred at 5005, 5890, 6310, and 6710 Å, respectively, giving access to lines of Mg, Al, Si, Ca, Ti, Fe, and Ni (Fig. 1). We also obtained the solar spectrum reflected by the asteroid Vesta with the same instrumental setup. Per filter and per star, we collected at least 3 exposures, resulting in total exposure times between 1.5 and 3 hours.

Data reduction was conducted following the standard procedures of IRAF: bias subtraction, flat-field correction, cosmic-ray removal, wavelength calibration through an internal UNe lamp, and, finally, continuum normalization. We then shifted all the spectra to the rest frame, using a degraded (to our resolution) version of the high-resolution spectrum of the Sun (Kurucz et al. 1984) as template. For each star (and filter) we co-added single exposures weighted by the S/N to obtain the final spectrum.

3 ABUNDANCES DETERMINATION

We determined the chemical abundances, through a local thermodynamic equilibrium (LTE) analysis, using the driver *abfind* of the February 2013 version of MOOG (Sneden 1973), which performs an adjustment of the abundance to match a single-line equivalent width (EW). MOOG requires a standard solar composition (we used the solar abundances of Grevesse & Sauval 1998), a model atmosphere, a line list, and an EW measurement to compute atomic abundances. Below we describe in detail each of these requirements.

3.1 Photospheric parameters and model atmospheres

In order to compute a model atmosphere the basic parameters are required: T_{eff} , $\log g$, $[\text{M}/\text{H}]$, and the microturbulence velocity (ξ). We adopted the T_{eff} , $\log g$, and $[\text{M}/\text{H}]$ values of our previous work (López-Valdivia et al. 2015). For ξ , we used the grid of atmospheric parameters of Takeda et al. (2005), which includes determination of T_{eff} , $\log g$, $[\text{M}/\text{H}]$, and ξ for 160 FGK stars. We looked within the Takeda’s grid the nearest set of the first 3 parameters for each star in our sample, and we assigned the Takeda’s determination of ξ to

our star. We found ξ values between 0.83 and 1.63 km s^{-1} , which are in agreement with values determined from synthetic spectra (Husser et al. 2013).

Regarding the atmospheric parameters uncertainties, we used those reported in López-Valdivia et al. (2015). For those cases where uncertainties were not available, we assigned, for $\log g$ and ξ , ± 0.27 dex and ± 0.27 km s^{-1} , as the typical uncertainty, which is the standard deviation of both $\log g$ and ξ distributions of the Takeda’s stars with T_{eff} within the values of our sample. For the uncertainty of $[\text{M}/\text{H}]$ we assumed ± 0.10 dex as a conservative error.

Using the atmospheric parameters reported in Table 1, we computed an ATLAS12 (Kurucz 2013) model atmosphere for each star; we also computed a solar model atmosphere with $T_{\text{eff},\odot}=5777$ K, $\log g_{\odot}=4.44$ dex, $[\text{M}/\text{H}]_{\odot}=0.0$ dex, and $\xi_{\odot}=1.0$ km s^{-1} .

3.2 Line list

We extracted the atomic transitions between 4995 and 6730 Å from The Vienna Atomic Line Database (VALD, Piskunov et al. 1995; Kupka et al. 1999), using the atmospheric parameters of the Sun. With these atomic transitions and the ATLAS12 solar model, we created with SYNTHE (Kurucz & Furenlid 1979; Kurucz & Avrett 1981; Kurucz 1993) a synthetic solar spectrum at the same spectral resolution as our observations. From the Vesta spectrum we selected 34 suitable atomic lines (listed in Table 2 and shown in Fig. 1) of 7 different chemical elements (Mg, Al, Si, Ca, Ti, Fe, and Ni), avoiding weak or saturated lines and blends.

Neves et al. (2009) pointed out that oscillator strengths ($\log gf$) of VALD might not be accurate enough for all the atomic transitions. To correct these possible inaccuracies, we determined the EW (see Section 3.3) for the 34 selected lines in the observed and synthetic solar spectrum; then, we compared both measurements and we modified the $\log gf$ until both measurements (observed and synthetic) agreed. For 15 lines, we also slightly modified the central wavelength reported by VALD. The transition parameters from VALD as well as their modifications are reported in Table 2.

3.3 Equivalent widths

The EW determination plays a fundamental role in the abundance determination. Since the EW depends strongly on the local continuum level, it is of crucial importance to determine it as accurately as possible. We implemented the following procedure to establish the local continuum level and to measure the EW.

First, by means of a Gaussian fit of a small region (5 Å), we identified and removed the points that form the spectral line of interest, which are points enclosed in a interval of $\pm 3\sigma$ from the central wavelength of the line. Then, we passed through an iterative routine the remaining spectrum, which is a combination of neighbouring lines and noise, to remove points above $\pm 2\sigma$ their average value in order to identify the local continuum. Finally, we adjusted to the line a Gaussian profile whose integral represents its EW.

We estimated the error on the EW applying a Monte Carlo method with 1000 iterations, randomly adding to the spectrum the noise of the local continuum.

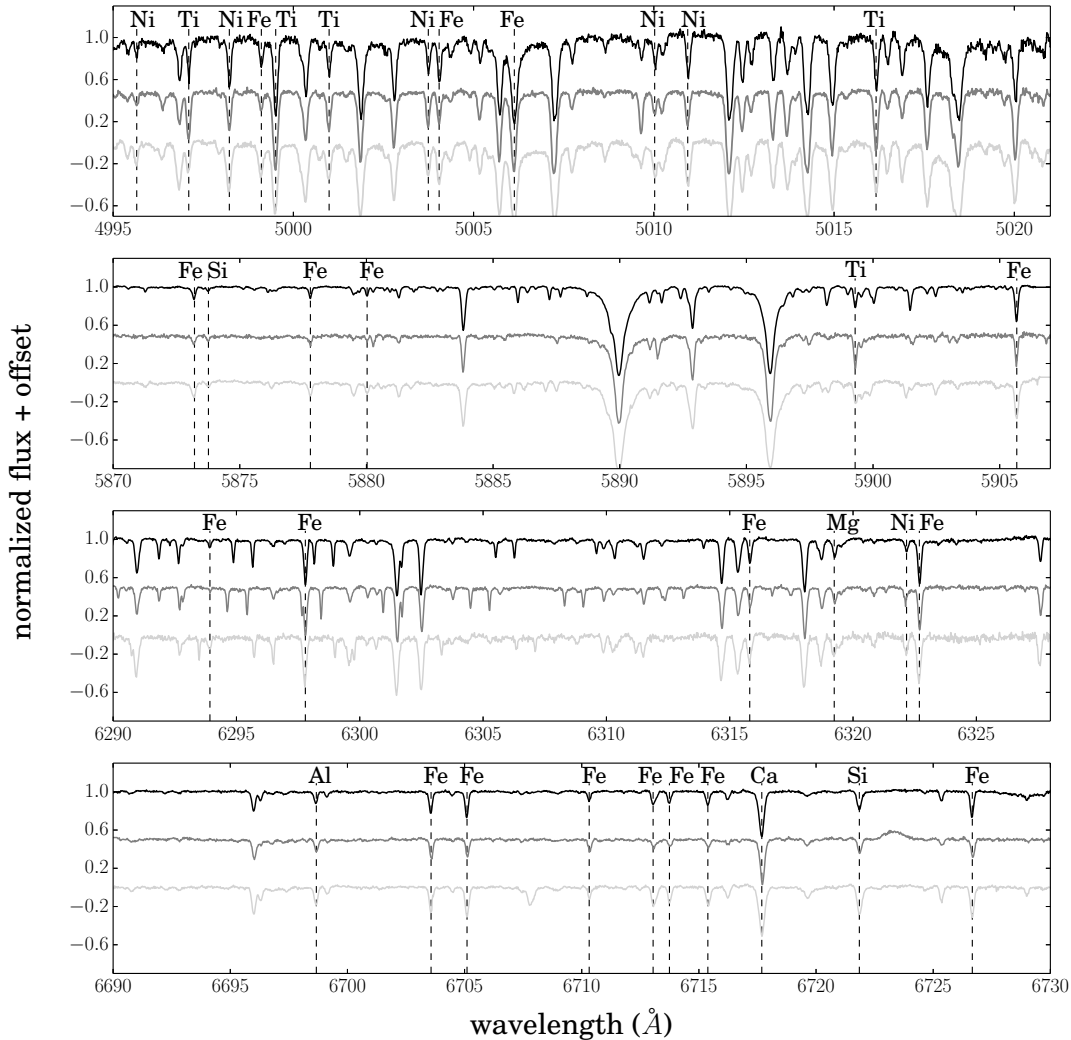


Figure 1. Normalized spectra of Vesta (black), HD 12699 (gray), and BD+28 3198 (light gray) in the four spectral regions, with identification of the atomic lines used to compute abundances. Note that the interval centred at 6310 Å is more affected by the presence of telluric lines.

We checked the consistency of our procedure by means of a comparison of solar line EWs determined in two different works (Neves et al. 2009; Takeda et al. 2005) with those determined by us. We measured in the solar spectrum of Kurucz et al. (1984), also used by Takeda and Neves, the EW for 57 and 178 iron lines reported by Takeda et al. 2005 and Neves et al. 2009, respectively. From this comparison, which is depicted in Fig. 2, we found good agreement, with some small differences, which can be explained by different local continuum levels.

3.4 Abundances computation and error budget.

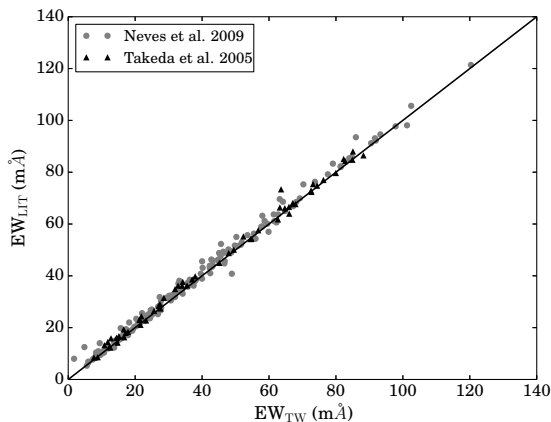
For each star and Vesta, we measured the EW of all lines listed in Table 2. We rejected, through visual inspection,

the lines whose best fit was not accurate enough; these lines vary from star to star. The EWs of Table 3 were used in MOOG to compute the chemical abundances. For species with more than one analysed transition, we carried out a weighted mean to obtain the final abundance, after having discarded outliers with an iterative 3σ clipping.

It is important to note that these two rejection processes could introduce potential biases and different abundance scales in stars with different excluded lines. The first filter is actually a visual inspection that relies on the S/N of the spectra and is not directly associated with abundances, while the sigma clipping is indeed applied directly to abundances, but it was employed in only one Fe line of eight stars. In order to take into account these potential biases, we conducted a Monte Carlo procedure

Table 1. Atmospheric parameters and their uncertainties of the stellar sample. For all the stars of our sample the error on the microturbulence velocity is 0.27 km s^{-1} .

Object	V	SType	T_{eff} (K)	σ (K)	$\log g$ (dex)	σ (dex)	[M/H] (dex)	σ (dex)	ξ (km s^{-1})
HD 5649	8.70	G0V	5830	52	4.45	0.22	-0.08	0.04	1.03
BD+60 402	10.26	G0V	5985	72	4.30	0.40	0.22	0.09	1.15
HD 16894	8.02	G2V	5500	70	4.05	0.30	-0.10	0.09	0.83
BD+60 600	8.65	G0V	5655	47	3.95	0.20	0.20	0.07	1.18
HD 232824	9.52	G2V	5900	67	4.15	0.35	0.16	0.08	1.27
HD 237200	9.66	G0V	6045	55	4.25	0.32	0.18	0.05	1.26
HD 26710	7.18	G2V	5815	47	4.55	0.20	-0.04	0.04	1.63
HD 31867	8.05	G2V	5590	57	4.40	0.25	-0.10	0.06	0.98
HD 33866	7.87	G2V	5481	123	4.33	0.27	-0.07	0.10	0.91
HD 41708	8.03	G0V	5998	58	4.55	0.27	0.08	0.10	1.33
HD 42802	6.44	G2V	5617	80	4.53	0.27	-0.11	0.10	0.98
HD 77730	7.39	G2V	5698	80	4.13	0.27	-0.05	0.10	1.00
HD 110882	8.87	G1V	5880	50	4.40	0.25	-0.28	0.04	1.14
HD 110884	9.11	G3V	5905	87	4.30	0.40	-0.26	0.08	1.16
HD 111513	7.35	G1V	5723	80	4.31	0.27	0.12	0.10	1.21
HD 111540	9.54	G1V	5840	47	4.20	0.25	0.14	0.05	1.13
HD 124019	8.56	G2V	5685	57	4.65	0.25	-0.18	0.06	0.88
HD 126991	7.90	G2V	5360	107	3.15	0.40	-0.34	0.14	1.27
HD 129357	7.83	G2V	5775	52	4.30	0.22	-0.14	0.05	1.21
HD 130948	5.88	F9IV-V	5885	80	4.42	0.27	-0.09	0.10	1.28
HD 135145	8.35	G0V	5997	80	4.14	0.27	-0.02	0.10	1.19
HD 135633	8.46	G0V	6095	67	4.25	0.40	0.22	0.06	1.27
HD 140385	8.57	G2V	5735	60	4.60	0.27	-0.16	0.08	1.13
HD 145404	8.54	G0V	5920	82	4.43	0.27	-0.16	0.10	1.20
HD 152264	7.74	G0V	6177	73	4.09	0.27	0.02	0.10	1.36
BD+29 2963	8.42	G0V	5865	55	4.70	0.22	0.00	0.04	1.27
HD 156968	7.97	G0V	6105	96	4.42	0.27	-0.03	0.10	1.30
HD 168874	7.01	G2IV	5696	80	4.41	0.27	-0.05	0.10	0.86
BD+28 3198	8.66	G2V	5840	35	4.00	0.17	0.24	0.05	1.25
TYC 2655-3677-1	9.93	G0V	6220	47	4.15	0.27	0.28	0.05	1.31
HD 333565	8.75	G1V	5990	52	4.45	0.27	0.12	0.05	1.19
HD 228356	9.07	G0V	6055	37	4.00	0.20	0.16	0.05	1.41
HD 193664	5.93	G3V	5942	112	4.47	0.27	-0.11	0.10	1.28
BD+47 3218	8.70	G0V	6050	52	4.05	0.30	0.16	0.06	1.41
HD 210460	6.19	G0V	5357	80	3.58	0.27	-0.17	0.10	1.27
TYC 3986-3381-1	10.37	G2V	5855	57	4.15	0.25	0.26	0.07	1.15
HD 212809	8.64	G2V	5975	55	4.55	0.27	0.16	0.05	1.33
BD+28 4515	8.73	G2V	5580	40	3.50	0.17	-0.22	0.06	1.29

**Figure 2.** Comparison of the solar EW computed in this study (EW_{TW}) and those determined by Takeda et al. (2005) and Neves et al. (2009).

in which we computed the Fe, Ni, and Ti abundance (elements with more available lines within our line list with 18, 6, and 5, respectively) for Vesta and some stars of our sample. We computed the mean abundance of Fe, Ni, and Ti using different size sets of randomly selected lines. After 1000 iterations for each set, element, and star, we demonstrated that the final abundance of these elements in all the cases does not change by more than 0.02 dex on average.

We report in Table 4 the abundances of the 7 atomic elements for our sample; they are given with respect to the solar abundances determined for Vesta² (see Table 5). The Table also provides the abundance uncertainty and the number of lines used for the abundance determination.

² $[X/H] = A(X)_{\text{star}} - A(X)_{\odot}$, where $A(X)_{\odot}$ is the computed abundance for Vesta.

Table 2. Set of atomic parameters from VALD and the modifications made by us to the central wavelength and the $\log gf$.

λ (Å)	$\Delta \lambda$ (Å)	element	χ (eV)	$\log gf$	$\Delta \log gf$
4995.650	0.005	Ni I	3.635	-1.580	-0.308
4997.098	-	Ti I	0.000	-2.070	-0.156
4998.224	-	Ni I	3.606	-0.700	-0.261
4999.112	-	Fe I	4.186	-1.740	-0.066
4999.503	0.007	Ti I	0.826	0.320	-0.279
5000.990	0.002	Ti I	1.997	-0.020	-0.255
5003.741	0.003	Ni I	1.676	-3.070	-0.265
5004.044	-	Fe I	4.209	-1.400	-0.110
5006.119	0.011	Fe I	2.833	-0.638	-0.336
5010.023	-	Ni I	3.768	-0.980	-0.085
5010.938	0.002	Ni I	3.635	-0.870	-0.161
5016.161	0.004	Ti I	0.848	-0.480	-0.294
5873.212	-	Fe I	4.256	-2.140	0.168
5873.763	-	Si I	4.930	-4.244	1.194
5877.788	-	Fe I	4.178	-2.230	-0.009
5880.027	-	Fe I	4.559	-1.940	-0.028
5899.293	-	Ti I	1.053	-1.100	-0.098
5905.671	0.003	Fe I	4.652	-0.730	-0.179
6293.925	-	Fe I	4.835	-1.717	-0.083
6297.792	0.002	Fe I	2.223	-2.740	-0.185
6315.811	-	Fe I	4.076	-1.710	-0.023
6319.237	-	Mg I	5.108	-2.324	0.238
6322.166	0.003	Ni I	4.154	-2.426	1.267
6322.685	0.004	Fe I	2.588	-1.170	-1.256
6698.673	-	Al I	3.143	-1.647	-0.255
6703.566	0.003	Fe I	2.759	-3.160	0.097
6705.101	0.003	Fe I	4.607	-1.392	0.269
6710.318	-	Fe I	1.485	-4.880	0.036
6713.046	-	Fe I	4.607	-0.963	-0.380
6713.743	-	Fe I	4.796	-1.600	0.186
6715.382	-	Fe I	4.608	-1.640	0.109
6717.681	0.003	Ca I	2.709	-0.524	0.025
6721.848	-	Si I	5.863	-1.527	0.415
6726.666	0.003	Fe I	4.607	-1.133	0.078

Along with the uncertainty on the EW measurement, the error on the stellar parameters is the source that most affects the final abundances. To properly assess it, we constructed a small matrix of abundance variations as a function of the difference in four atmospheric parameters (T_{eff} , $\log g$, $[M/H]$, and ξ), taking the solar values as reference. For each absorption line j , we considered the EW measured on the Vesta spectrum and we computed a grid of abundance variations $\Delta[X/H]_j = [X/H]_j - [X/H]_{j,\odot}$, caused by a difference $\Delta T_{\text{eff},\odot} = 150$ K, of $\Delta \log g_{\odot} = 0.40$ dex, of $\Delta[M/H]_{\odot} = 0.20$ dex, and of $\Delta \xi_{\odot} = 0.50$ km s $^{-1}$. Then, for each star, we obtained the $\Delta[X/H]_j$ corresponding to each atmospheric parameter by linearly interpolating this grid, assuming, as parameter value difference, the errors reported in Table 1. The error on the abundance derived from each absorption line is the quadratic sum of the error on the atmospheric parameters and the EW.

Table 3. EWs of the atomic lines considered for abundance determination. The complete Table is available in electronic version.

Star	λ (Å)	Ele.	EW (mÅ)	σ (mÅ)
HD 5649	4998.224	28	27.35	2.51
HD 5649	4999.510	22	59.01	2.77
HD 5649	5000.992	22	24.08	3.18
HD 5649	5006.130	26	124.59	5.58
HD 5649	5010.940	28	23.02	2.81
HD 5649	5016.165	22	24.09	3.35
HD 5649	5877.788	26	8.71	1.16
HD 5649	5880.027	26	10.47	1.57
HD 5649	5905.674	26	30.81	1.62
HD 5649	6297.794	26	47.92	1.26
HD 5649	6322.689	26	49.03	1.82
...

4 DISCUSSION

4.1 Super metal rich stars and the [Ref] index

In our working sample, we included 11 stars considered as SMR ($[M/H] \geq 0.16$ dex) in López-Valdivia et al. (2014). From the present high-resolution analysis, we confirm the SMR status, by means of their iron abundance, for 6 objects, namely BD+60 402, BD+60 600, HD 237200, HD 135633, BD+28 3198, and TYC 3986-3381-1, while, for other 3 stars (BD+47 3218, HD 212809, HD 232824), we obtain $[Fe/H]$ lower than the SMR threshold. However, both BD+47 3218 and HD 212809 have super-solar abundances for all atomic species and some of them are well above the +0.16 dex threshold. The two remaining cases of SMR stars, HD 228356 and TYC 2655-3677-1, are discussed below.

The 6 SMR stars are therefore excellent targets to search for giant planet companions. In order to quantify the probability of detecting these planets, we make use of the [Ref] index defined by Gonzalez (2009):

$$[\text{Ref}] = \log \left(24 \times 10^{7.55+[Mg/H]} + 28 \times 10^{7.53+[Si/H]} + 56 \times 10^{7.47+[Fe/H]} \right) - 9.538 \quad (1)$$

We report the [Ref] index and $[Fe/H]$ in Table 6, where we also provide the probability $[P(\%)]$ of hosting a giant planet, obtained from the probability functions of Gonzalez (2014) and Fischer & Valenti (2005), based solely on chemical composition considerations. BD+60 600 (39%) and BD+28 3198 (22%) stand out as the best targets for a giant exoplanet search program.

4.2 $[X/Fe]$ behaviour and comparison with literature data.

In Figure 5, we show the $[X/Fe]$ ratios for the elements included in our analysis. In order to check for consistency with other abundance studies on objects of the solar neighbourhood, we compare our results with the works of Neves et al. (2009), Adibekyan et al. (2012), and Hinkel et al. (2014), which include LTE abundances for FGKM main sequence stars, within a distance of 150 pc from the Sun. We found good agreement with these previous works. Our Mg, Si, Ca and Ti ratios present a higher scatter than Al, and Ni, nev-

Table 4. Chemical abundances of the stellar sample. For each element we present in different rows the weighted mean abundance, its error, and the number of lines used in the determination of the abundance per star.

Star	[Mg/H]	[Al/H]	[Si/H]	[Ca/H]	[Ti/H]	[Fe/H]	[Ni/H]
HD 5649	–	–	–	-0.48	-0.42	-0.32	-0.43
	–	–	–	0.13	0.07	0.02	0.06
	–	–	–	1	3	9	2
BD+60 402	+0.18	+0.20	+0.20	+0.26	+0.17	+0.19	+0.16
	0.12	0.04	0.04	0.19	0.06	0.02	0.04
	1	1	1	1	4	15	5
HD 16894	-0.21	–	+0.25	+0.32	+0.07	+0.04	-0.01
	0.05	–	0.08	0.17	0.06	0.02	0.04
	1	–	1	1	4	16	6
BD+60 600	+0.51	+0.39	+0.44	+0.51	+0.24	+0.35	+0.34
	0.05	0.04	0.04	0.13	0.05	0.01	0.03
	1	1	2	1	4	18	5
HD 232824	-0.07	-0.08	-0.03	-0.07	-0.24	-0.09	-0.06
	0.07	0.05	0.04	0.17	0.07	0.02	0.04
	1	1	2	1	4	17	4
HD 237200	+0.03	+0.13	+0.20	+0.27	+0.21	+0.18	+0.14
	0.07	0.04	0.04	0.17	0.07	0.01	0.04
	1	1	2	1	4	16	5
HD 26710	-0.13	–	+0.09	+0.08	-0.23	+0.08	-0.12
	0.04	–	0.04	0.13	0.05	0.01	0.03
	1	–	1	1	4	14	4
HD 31867	-0.21	–	+0.13	-0.06	-0.13	-0.07	-0.05
	0.04	–	0.05	0.14	0.04	0.01	0.03
	1	–	1	1	5	14	6
HD 33866	-0.06	–	–	+0.04	-0.35	-0.22	-0.20
	0.06	–	–	0.17	0.08	0.02	0.04
	1	–	–	1	4	15	5
HD 41708	+0.22	–	–	-0.03	+0.07	+0.08	+0.12
	0.04	–	–	0.16	0.05	0.01	0.03
	1	–	–	1	4	15	6
HD 42807	+0.02	–	+0.03	+0.06	-0.05	-0.10	-0.15
	0.04	–	0.06	0.16	0.05	0.01	0.04
	1	–	1	1	5	15	5
HD 77730	-0.50	-0.18	-0.15	-0.30	-0.41	-0.40	-0.35
	0.06	0.05	0.04	0.16	0.06	0.02	0.04
	1	1	1	1	5	16	6
HD 110882	-0.32	–	–	-0.31	-0.18	-0.37	-0.31
	0.04	–	–	0.14	0.05	0.02	0.04
	1	–	–	1	4	9	6
HD 110884	–	-0.17	–	-0.11	-0.18	-0.14	-0.11
	–	0.04	–	0.19	0.07	0.02	0.05
	–	1	–	1	3	16	4
HD 111513	+0.23	+0.03	+0.21	+0.08	-0.03	+0.04	+0.12
	0.04	0.04	0.03	0.16	0.06	0.01	0.03
	1	1	2	1	4	17	5
HD 111540	+0.00	+0.17	+0.28	+0.24	+0.09	+0.13	+0.14
	0.09	0.04	0.04	0.14	0.05	0.01	0.04
	1	1	2	1	4	15	6
HD 124019	-0.16	-0.15	+0.30	-0.17	-0.12	-0.05	-0.24
	0.06	0.04	0.06	0.14	0.05	0.01	0.04
	1	1	1	1	5	13	5
HD 126991	-0.29	-0.20	-0.41	-0.20	-0.10	-0.53	-0.37
	0.04	0.04	0.04	0.20	0.06	0.02	0.04
	1	1	1	1	5	16	5
HD 129357	-0.04	-0.01	–	-0.03	+0.02	-0.01	-0.01
	0.04	0.03	–	0.13	0.04	0.01	0.03
	1	1	–	1	5	16	6
HD 130948	-0.08	–	+0.11	-0.10	-0.28	-0.11	-0.14
	0.04	–	0.06	0.16	0.08	0.02	0.04
	1	–	1	1	3	15	3
HD 135145	-0.19	–	–	-0.11	+0.00	-0.03	+0.03
	0.04	–	–	0.16	0.06	0.02	0.03
	1	–	–	1	4	15	6

Table 4 – *continued*

Star	[Mg/H]	[Al/H]	[Si/H]	[Ca/H]	[Ti/H]	[Fe/H]	[Ni/H]
HD 135633	+0.02	+0.14	+0.29	+0.33	+0.14	+0.23	+0.13
	0.06	0.04	0.08	0.19	0.06	0.01	0.04
	1	1	1	1	4	15	5
HD 140385	+0.01	-0.03	-0.11	-0.28	+0.12	-0.24	-0.15
	0.05	0.04	0.04	0.15	0.05	0.01	0.03
	1	1	2	1	5	16	6
HD 145404	-0.25	-0.25	–	-0.23	-0.08	-0.18	-0.19
	0.04	0.04	–	0.16	0.05	0.01	0.04
	1	1	–	1	5	16	6
HD 152264	-0.11	+0.00	+0.03	+0.16	+0.17	+0.07	+0.10
	0.04	0.04	0.04	0.16	0.06	0.01	0.03
	1	1	2	1	4	17	5
BD+29 2963	-0.17	-0.16	-0.28	-0.30	-0.08	-0.22	-0.23
	0.04	0.04	0.04	0.13	0.04	0.01	0.04
	1	1	1	1	5	17	5
HD 156968	+0.00	-0.11	–	-0.03	+0.06	-0.03	-0.02
	0.05	0.04	–	0.16	0.06	0.02	0.04
	1	1	–	1	5	16	6
HD 168874	+0.00	+0.03	+0.05	+0.00	+0.04	-0.01	+0.07
	0.05	0.04	0.08	0.16	0.06	0.02	0.04
	1	1	1	1	5	15	4
BD+28 3198	+0.44	+0.30	+0.35	+0.46	+0.33	+0.27	+0.36
	0.04	0.04	0.04	0.12	0.04	0.01	0.03
	1	1	2	1	4	18	5
HD 333565	-0.19	-0.05	-0.02	-0.16	+0.12	-0.03	+0.04
	0.04	0.04	0.03	0.15	0.06	0.01	0.04
	1	1	1	1	4	13	3
HD 193664	-0.26	–	+0.09	-0.02	-0.17	-0.12	-0.06
	0.05	–	0.08	0.17	0.09	0.02	0.04
	1	–	1	1	3	16	5
BD+47 3218	+0.06	+0.09	+0.15	+0.28	+0.24	+0.13	+0.32
	0.04	0.04	0.04	0.16	0.06	0.01	0.03
	1	1	2	1	4	15	5
HD 210460	-0.49	–	–	-0.54	-0.38	-0.37	-0.37
	0.05	–	–	0.17	0.06	0.02	0.04
	1	–	–	1	4	13	5
TYC 3986-3381-1	–	+0.38	+0.48	+0.40	+0.29	+0.32	+0.23
	–	0.05	0.04	0.15	0.07	0.01	0.04
	0	1	1	1	4	14	4
HD 212809	+0.01	–	–	+0.28	+0.03	+0.08	+0.08
	0.07	–	–	0.15	0.05	0.01	0.04
	1	–	–	1	4	15	5
BD+28 4515	+0.02	–	+0.38	+0.24	-0.10	+0.07	+0.10
	0.04	–	0.05	0.13	0.05	0.01	0.03
	1	–	1	1	4	17	6

ertheless, this pattern is also present in the comparison sample.

The errors in the Ca abundance are, on average, larger than for the other elements and always higher than 0.10 dex. This anomaly is due to fact that the Ca abundance is very sensitive to the error in surface gravity: in fact, we found that $\sigma_{\log g} = 0.20$ dex produces a difference of 0.08 dex in the Ca abundance, while for the other elements the uncertainty in $\log g$ does not affect much the overall error.

We found 8 of our stars in the Hypatia catalogue, a compilation of chemical abundances from high-resolution spectroscopy (Hinkel et al. 2014), and 2 objects are also present in the more recent work by Mahdi et al. (2016). We found a maximum (minimum) difference of +0.20 dex (-0.02 dex) between our abundances and those of Hinkel et al. (2014).

This discrepancy is as large as the typical dispersion among catalogues included in Hinkel et al. (2014). As an example, in Fig. 3, we show the comparison of our [Fe/H] values and those of Hypatia for the the stars HD 41708, HD 42807, HD 111513, HD 129357, HD 140385, and HD 156968; we also include the iron abundance of Mahdi et al. (2016) for HD 42807 and HD 111513. If we take into account that the solar scale of Lodders et al. (2009), used as reference by Hinkel et al. (2014), has a iron abundance 0.05 dex lower than in Grevesse & Sauval (1998), the agreement with our results improves.

Mahdi et al. (2016) provide the abundance of Si, Ca, Ti, Fe, and Ni for the stars HD 42807 and HD 111513. We found a difference with our results between +0.08 and +0.11 dex for HD 42807 and in the interval -0.15 to +0.07 dex for

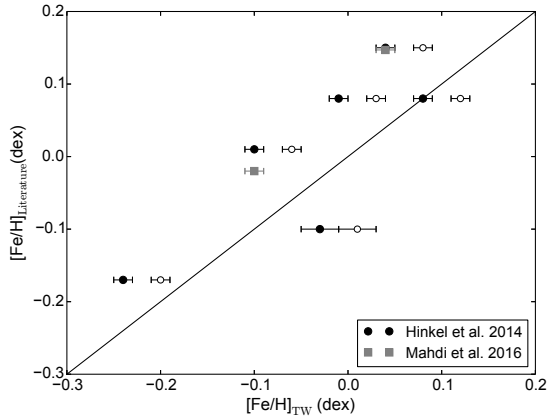


Figure 3. Comparison of our iron abundances and those of Hinkel et al. (2014) (filled circles) and Mahdi et al. (2016) (filled squares). The empty circles represent the transformation of our iron abundances to the Hinkel et al. (2014) reference solar abundances.

Table 5. Solar abundances from Vesta spectrum and the values of Grevesse & Sauval (1998).

Element	Vesta	G&S
Mg	7.54 ± 0.02	7.58 ± 0.05
Al	6.46 ± 0.02	6.47 ± 0.07
Si	7.52 ± 0.02	7.55 ± 0.05
Ca	6.38 ± 0.09	6.36 ± 0.02
Ti	4.98 ± 0.03	5.02 ± 0.06
Fe	7.49 ± 0.01	7.50 ± 0.05
Ni	6.23 ± 0.02	6.25 ± 0.04

HD 111513. Such values, although larger than our errors, can be explained by systematic differences, such as different *log gf* values or different atmospheric parameters adopted.

4.3 Stars with broad line profiles

Two stars, TYC 2655-3677-1 and HD 228356, show line profiles which are significantly broader than the rest of the sample (see Fig. 4). This is due to relatively high rotational velocity (with a possible significant contribution by macroturbulence). These two objects also have high lithium abundance ($A(\text{Li})=2.54$ for TYC 2655-3677-1 and HD 228653 of $A(\text{Li})=2.71$; López-Valdivia et al. 2015), indicating that they are probably young stars.

Their line profiles, however, are broad enough to make very difficult to identify isolated, un-blended lines for a correct abundance measurement. We have therefore excluded the two stars from our abundance analysis. We measured the FWHM and we computed, using eq. 6 of Strassmeier et al. (1990), the projected rotation velocity ($v \sin i$) for 6 atomic lines in the region around 6710 Å.

We assumed a macroturbulence velocity of 3 km s^{-1} and an instrumental FWHM = 0.19 Å and we obtained $v \sin i = 8.5$ and 9.7 km s^{-1} for TYC 2655-3677-1 and HD 228653, respectively.

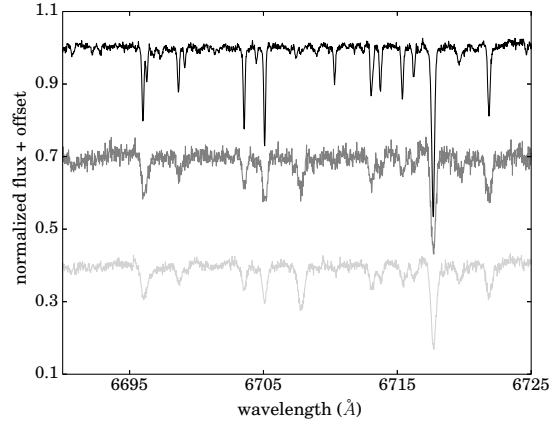


Figure 4. The spectra of TYC 2655-3677-1 (gray), and HD 268356 (light gray), compared with the spectrum of Vesta (black).

Table 6. Probability of hosting a giant planet using $[\text{Fe}/\text{H}]$ and the $[\text{Ref}]$ index.

Object	$[\text{Fe}/\text{H}]$	$\mathcal{P}(\%)$	$[\text{Ref}]$	$\mathcal{P}(\%)$
HD 5649	-0.32	0	–	–
BD+60 402	+0.19	7	+0.19	8
HD 16894	+0.04	3	+0.07	3
BD+60 600	+0.35	15	+0.42	39
HD 232824	-0.09	1	-0.07	1
HD 237200	+0.18	6	+0.15	6
HD 26710	+0.08	4	+0.04	2
HD 31867	-0.07	2	-0.03	1
HD 33866	-0.22	1	–	–
HD 41708	+0.08	4	–	–
HD 42807	-0.10	1	-0.03	1
HD 77730	-0.40	0	-0.33	0
HD 110882	-0.37	0	–	–
HD 110884	-0.14	1	–	–
HD 111513	+0.04	3	+0.14	5
HD 111540	+0.13	5	+0.15	6
HD 124019	-0.05	2	+0.06	3
HD 126991	-0.53	0	-0.43	0
HD 129357	-0.01	2	+0.09	4
HD 130948	-0.11	1	-0.03	1
HD 135145	-0.03	2	–	–
HD 135633	+0.23	8	+0.21	9
HD 140385	-0.24	0	-0.13	0
HD 145404	-0.18	1	–	–
HD 152264	+0.07	4	+0.02	2
BD+29 2963	-0.22	1	-0.22	0
HD 156968	-0.03	2	–	–
HD 168874	-0.01	2	+0.01	2
BD+28 3198	+0.27	10	+0.34	22
HD 333565	-0.03	2	-0.06	1
HD 193664	-0.12	1	-0.08	1
BD+47 3218	+0.13	5	+0.12	5
HD 210460	-0.37	0	–	–
TYC 3986-3381-1	+0.32	13	–	–
HD 212809	+0.08	4	–	–
BD+28 4515	+0.07	4	+0.17	7

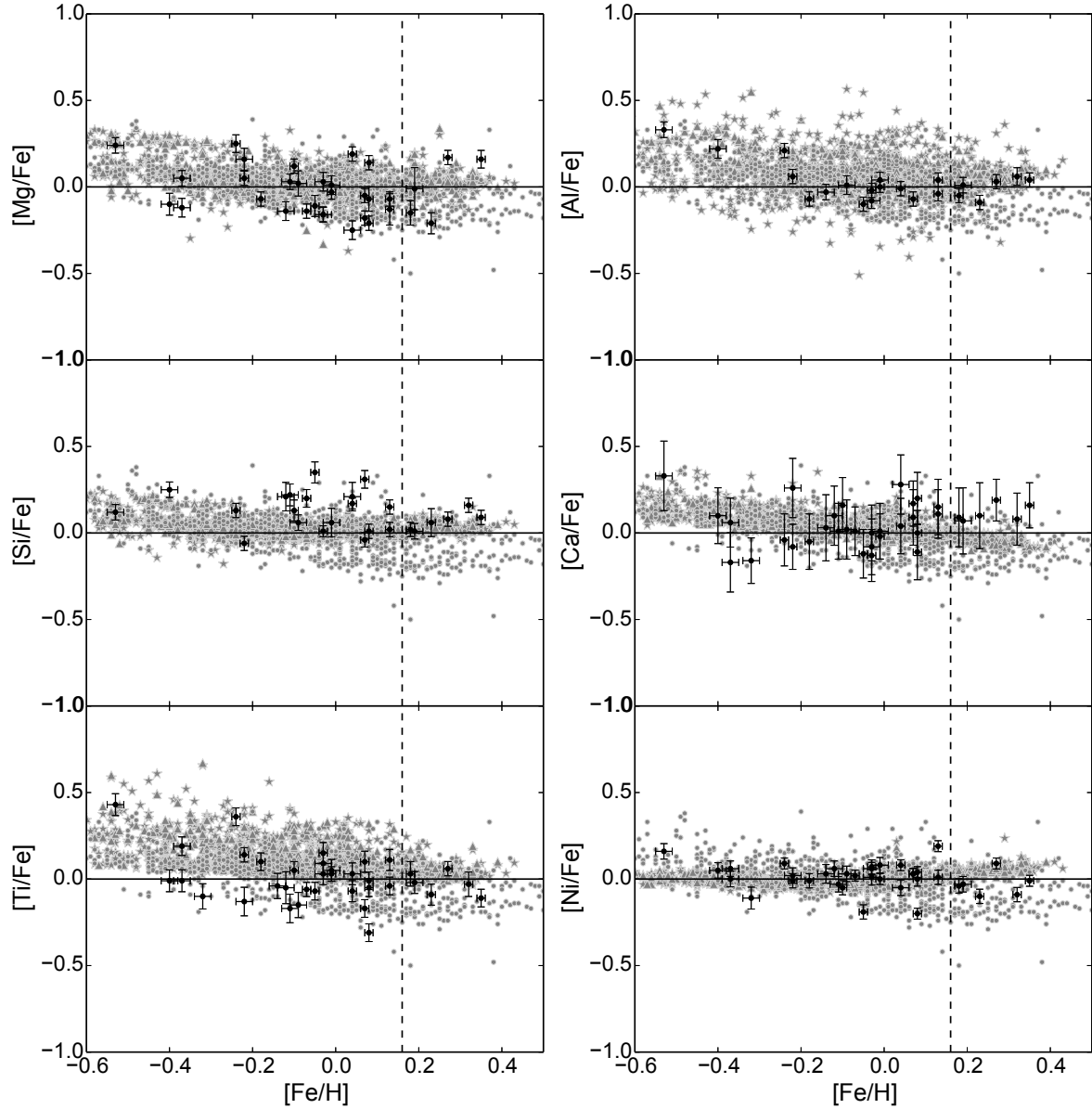


Figure 5. $[X/Fe]$ vs $[Fe/H]$ ratio for our sample (black circles), Neves et al. (2009)(gray triangles), Adibekyan et al. (2012) (gray stars), and for Hinkel et al. (2014) (gray circles). The vertical dashed line indicates the super metallicity threshold.

ACKNOWLEDGEMENTS

This research has made use of the SIMBAD data base, operated at CDS, Strasbourg, France. The authors would like to thank CONACyT for financial support through grants CB-2011-169554 and CB-2015-256961. This research has made use of the SIMBAD data base, operated at CDS, Strasbourg, France.

REFERENCES

- Adibekyan, V. Z., Sousa, S. G., Santos, N. C., et al. 2012, *A&A*, 545, A32
- Alibert, Y., Mordasini, C., & Benz, W. 2004, *A&A*, 417, L25
- Bush, T. C., & Hintz, E. G. 2008, *AJ*, 136, 1061
- Casagrande, L., Schönrich, R., Asplund, M., et al. 2011, *A&A*, 530, A138
- Castelli, F., & Kurucz, R. L. 2003, *Modelling of Stellar*

- Atmospheres, IAU Symp., 210, 20P
ESA 1997, ESA Special Publication, 1200,
Fischer, D. A., & Valenti, J. 2005, *ApJ*, 622, 1102
Gonzalez, G. 1997, *MNRAS*, 285, 403
Gonzalez, G. 2009, *MNRAS*, 399, L103
Gonzalez, G. 2014, *MNRAS*, 443, 393
Grevesse, N., & Sauval, A. J. 1998, *Space Sci. Rev.*, 85, 161
Hinkel, N. R., Timmes, F. X., Young, P. A., Pagano, M. D.,
& Turnbull, M. C. 2014, *Aj*, 148, 54
Husser, T.-O., Wende-von Berg, S., Dreizler, S., et al. 2013,
A&A, 553, A6
Kupka, F., Piskunov, N., Ryabchikova, T. A., Stempels,
H. C., & Weiss, W. W. 1999, *A&AS*, 138, 119
Johnson, J. A., Aller, K. M., Howard, A. W., & Crepp,
J. R. 2010, *PASP*, 122, 905
Kurucz, R. 1993, SYNTHE Spectrum Synthesis Programs
and Line Data. Kurucz CD-ROM No. 18. Cambridge,
Mass.: Smithsonian Astrophysical Observatory, 1993., 18,
Kurucz, R. L. 2013, Astrophysics Source Code Library,
ascl:1303.024
Kurucz, R. L., & Avrett, E. H. 1981, SAO Special Report,
391, 391
Kurucz, R. L., & Furenlid, I. 1979, SAO Special Report,
387, 387
Kurucz, R. L., Furenlid, I., Brault, J., & Testerman, L.
1984, National Solar Observatory Atlas, Sunspot, New
Mexico: National Solar Observatory, 1984,
Lodders, K., Palme, H., & Gail, H.-P. 2009, Landolt
Börnstein,
López-Valdivia, R., Bertone, E., Chávez, M., et al. 2014,
MNRAS, 444, 2251
López-Valdivia, R., Hernández-Águila, J. B., Bertone, E.,
et al. 2015, *MNRAS*, 451, 4368
Mahdi, D., Soubiran, C., Blanco-Cuaresma, S., & Chemin,
L. 2016, *A&A*, 587, A131
Mayor, M., & Queloz, D. 1995, *Nature*, 378, 355
Neves, V., Santos, N. C., Sousa, S. G., Correia, A. C. M.,
& Israelian, G. 2009, *A&A*, 497, 563
Pollack, J. B., Hubickyj, O., Bodenheimer, P., et al. 1996,
Icarus, 124, 62
Piskunov, N. E., Kupka, F., Ryabchikova, T. A., Weiss,
W. W., & Jeffery, C. S. 1995, *A&AS*, 112, 525
Santos, N. C., Israelian, G., & Mayor, M. 2001, *A&A*, 373,
1019
Snedden, C.A. 1973, Ph.D. Thesis, University of Texas,
Austin
Sousa, S. G., Santos, N. C., Israelian, G., Mayor, M., &
Udry, S. 2011, *A&A*, 533, A141
Strassmeier, K. G., Fekel, F. C., Bopp, B. W., Dempsey,
R. C., & Henry, G. W. 1990, *ApJS*, 72, 191
Takeda, Y., Ohkubo, M., Sato, B., Kambe, E., & Sadakane,
K. 2005, *PASJ*, 57, 27